Hindawi
Geofluids
Volume 2022, Article ID 3910586, 11 pages
https://doi.org/10.1155/2022/3910586

Research Article

Characteristics of Middle-Lower Ordovician Ultradeeply Buried Carbonate Reservoirs in Shunbei Area, Tarim Basin—A Case Study from Well SHBP1

Xiao Chongyang,[1,2,3] Zhao Rui,[4] Fu Heng,[1,2] Huang Cheng,[3] Han Jun,[3] and Lin bo[3]

[1]*College of Energy, Chengdu University of Technology, 610059, China*
[2]*State Key Laboratory of Oil and Gas Reservoir Geology and Exploration, Chengdu, Sichuan 610059, China*
[3]*Northwest Oilfield Branch Company, SINOPEC, Urumqi 830011, China*
[4]*Petroleum Exploration and Production Research Institute, SINOPEC, Beijing 100083, China*

Correspondence should be addressed to Fu Heng; doublesun_show@163.com

Received 9 January 2022; Revised 14 February 2022; Accepted 16 February 2022; Published 15 March 2022

Academic Editor: Zheng Sun

Fracture-pore complexes, located at fault zones of Darriwilian carbonates, are the main exploration targets in the Shunbei area, Tarim Basin. This article focuses on the carbonate characteristics in the Lower Ordovician of Well ShunbeiPeng1 (SHBP1), the carbonate is sandwiched by two trending NW-SE deep-seated, strike-slip faults in the Shuntuoguole uplift. Based on detailed core investigation and careful petrographic examination, two main reservoir types, denoting microquartz and dolomite, are recognized. The former is mainly constrained in the lower part of the sampled core and gradually evolves to the latter with progressively decreases of silica. Integrated isotopic geochemistry (C, O, and Sr) and fluid inclusion microthermometry suggest that the fluids are hydrothermal origin and migrate along deep-seated strike-slip faults, forming favorable carbonate reservoirs. The fault-controlled hydrothermal reservoirs, characterized by the strong amplitude in the seismic profile, would be the most promising exploration area in deeply buried carbonates in the Tarim Basin, particularly in the Shuntuoguole area.

1. Introduction

The lower Paleozoic carbonate rocks, located at the Tarim Basin, contain abundant oil and gas resources and are the main targets for hydrocarbon exploration in the future [1, 2–6]. However, the characteristics, mechanism, and distribution of the promising carbonate reservoirs have not been clearly understood, probably due to the ultradeeply burial and multiple intensive tectonic alterations. As a result, it is urgent to perform investigations to reveal the inherent characteristics of ultradeeply buried carbonate reservoirs in Tarim Basin.

Shunbei area, located in the Shuntuoguole low uplift, is characterized with low exploration position. Notably, from the purpose of hydrocarbon exploration in Shunbei area, fault zone is the main target area [7–11]. Since the successive breakthrough of the Shunbei No. 1 Fault and subsequent No. 5, No. 7 Faults demonstrated the abundant distribution of fault-controlled carbonate reservoirs in the Middle Ordovician carbonates [12–16]. In light of abnormal beaded reflectors, the high-quality reservoirs may exist in the deep-buried geological layers, ranging from Florian to Dapingian successions [9, 17, 18]. However, these reservoirs have not yet been detailed studied, due to the scarcity of the drilling core dataset. Therefore, this article aims at determining the characteristics of the deep-burial carbonate reservoirs, and their relationships to the tectonic activity as well as evolution, and documents the main influential factors of these deep-burial carbonate reservoirs finally. In order to reach the goals, in this article, a systematic petrographic and geochemical study of Well SHBP1, located at the Lower Ordovician Yingshan Formation of the Middle Ordovician, is carried out, proving siliceous is of secondary metasomatism origin. The above observations further indicate that transformation

is important for the siliceous fluid reservoirs in this block. Till now, current investigation, upon Shunbei Yingshan Formation, is greatly limited as a result of low exploration and well coring data, therefore it is hard to judge the siliceous metasomatism of reservoirs, its function to transform the spatial distribution characteristics, and its scale. Accordingly, the study of the core of Well SHBP1 will be an important way to clarify the nature and source of siliceous fluid and serves as the prediction tool of the development characteristics, genesis, and main controlling factors of the fracture hydrothermal-controlled carbonate reservoir. This research will provide reference for future oil and gas exploration of deep-buried carbonate reservoirs.

2. Geological Setting

Shunbei area is located in the north of the Shuntuoguole low uplift, falling in the conjunction between the Awati faulted depression, Manjiaer depression, and Shaya uplift. The Shuntuoguole uplift formed in the middle Caledonian and underwent multiple tectonic activities, such as the Hercynian and Indo-china, forming the nowadays framework. A series of deep-seated and strike-slip faults, which intersect the strata from the crystalline basement through the Upper Ordovician Yijianfang Formation, are present in the Shuntuoguole uplift [7, 8, 19, 20]. The Cambrian-Lower Ordovician in the Shunbei area is dominated by huge thick carbonate rocks, and then, the craton disappeared. In the late Hercynian period, the northern Tianshan Ocean and the southern Tettis Ocean closed orogeny, and the Tarim block became the southern margin of the Eurasian continent, and the Marine sediments were dominated by the continental littoral shallow lake and fluvial facies. Under the control of oblique and rotating stress fields, generated by the multistage activities of the two paleo-uplifts in Tazhong and Tabei, a series of intraplate strike-slip fault zones, sharing a good matching relationship with regional tectonic events, formed in the Shuntuoguole area (Figure 1). Multistage fault zones, with NE and NW directions and large strike-slip features, are developed in the area, which cut down through the Cambrian to the basement and disappeared in the Upper Ordovician mudstone or Yijianfang Formation plastic formation [7, 8]. Notably, the vertical structure has upright or flower-like shape. Moreover, analysis results from multiple wells indicate the desirable reservoir-forming conditions in Shunbei area, and the fault zone is the main favorable area for hydrocarbon enrichment.

Well SHBP1 is sandwiched between No. 5 and No. 7 strike-slip fault zone, trending NW-SE direction, meanwhile it has negative flower structure and conjugates the NE-trending strike-slip faults in the Xayar uplift (Figure 1). In the block, there are different positions of deficiency in the middle and upper Silurian series, middle and lower Devonian series, upper Carboniferous series, lower and upper Permian series, Jurassic series, upper Cretaceous series, and Paleogene Kugelman formation, while the rest of strata are fully developed. In the block, the Ordovician strata are fully developed, including the lower series Penglaiba formation, the middle series Yingshan formation, the middle series Tongyi Jianfang formation, the upper series Qierbak formation, Lianglitage formation, and Sangtamu formation. Among them, the Tongjianfang formation and the Yingshan formation in the Ordovician system are the main target strata, and the Penglaiba formation-Yingshan formation developed NE concealed faults, and the reservoir type is fracture-cavity type.

3. Methods

The samples, for cathodoluminescence (CL) analysis, were processed by twin polishing, then pasted with epoxies, and tested with the help of CL8200 MK5 cathodoluminescence apparatus. The working conditions were set as high pressure at 8 ~ 10 kV, electric current at 0.4 ~ 0.6 mA, and vacuum degree at 13~7 Pa.

As for scanning electron microscope (SEM) analysis, fresh core samples were put in a 50°C oven for four hours at first and then coated with gold membrane. At room temperature, the samples were observed, using a Quanta 200 scanning electron microscope with frequency of 50 HZ and resolution of 30 nm.

In situ C-O isotope analysis was conducted on sections with thickness ranging from 50 to 100 μm, using laser Raman ablation on a Thermo Fisher MAT253 mass spectrometer. Specifically, the laser spot diameter is 200 μm, and GBW4405 and 811 standards are adopted for parallel analysis, with a resolution of ±0.22% for both $\delta^{13}C$ and $\delta^{18}O$ measurement.

Sr isotopic analysis was carried out on a Finnigan MAT-253 Triton TI mass spectrometer with an error of 0.002%. The samples for fluid inclusion analysis were prepared into 0.1 mm sections by twin polishing operation, and a Leica DM4500P microscope was employed for mineral observation. During a Linkam TS1400XY type cooling/heating stage, homogenization and freezing-point temperatures were measured, the resolutions can reach 2°C and 0.5 (±5%)°C, respectively.

3.1. Petrography Characteristics. The cores, sampling at the vicinity of the lower boundary of Yingshan Formation from Well SHBP1, which is the only cored individual well in study area, are badly damaged. The color of the whole rock is gray to white gray. From the bottom to the top, two units could be subdivided based on detailed core investigation as well as microscopic examination.

The lower unit, with color from light to gray, has a high content of silica with minor black quartz crystals (Figure 2(a)). The content of silica gradually decreases downwards, whereas the calcareous increases (Figure 2(b)). From a microscopic perspective, two distinctive quartz textures are recognized, suggesting the matrix and cement quartz (Figures 2(c) and 2(d)). The matrix quartz is mainly composed of microcrystalline quartz (Figures 2(e) and 2(f)) and chalcedony. The former is very small (<5 ~ 20 μm) with equigranularity structure, whereas the latter is fibrous and/or radial with cryptocrystalline texture. In contrast, the quartz cements commonly consist of coarse to very coarse crystalline (20~2000 μm), and its shape varies from blade to columnar

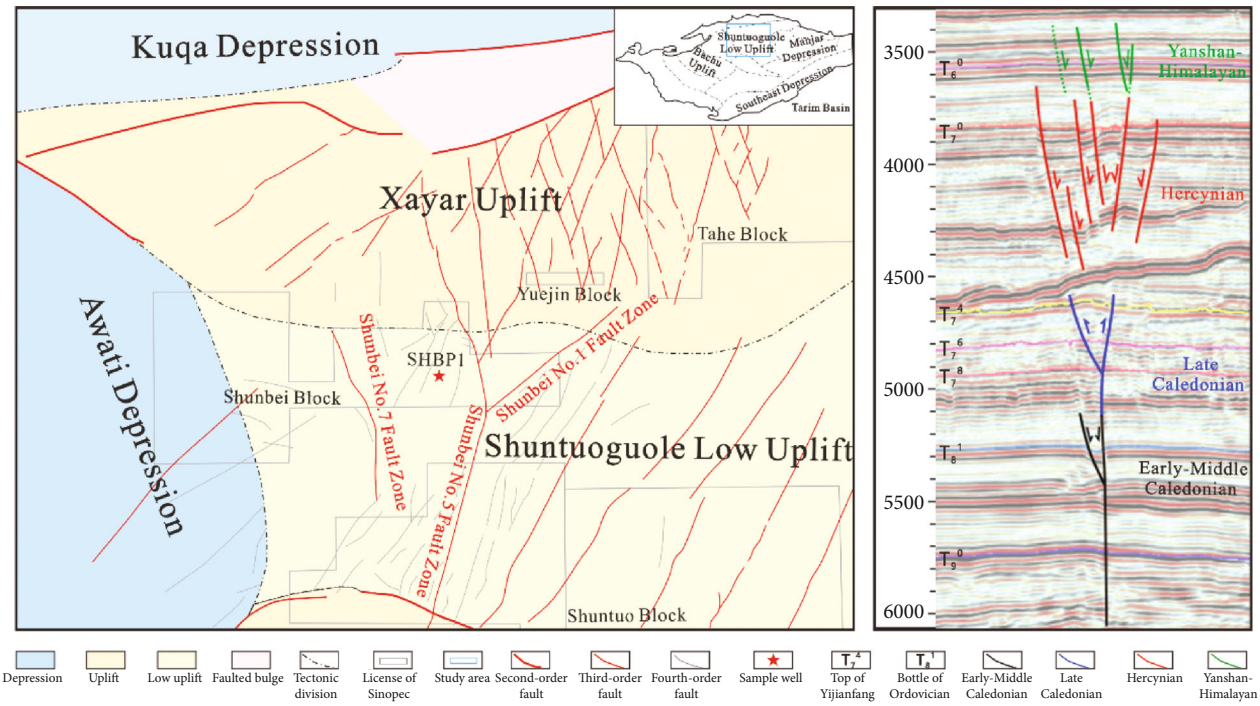

Figure 1: Tectonic location of Shunbei area in Tarim Basin.

forms (Figure 2(c)). In addition, crystals occur as fracture infills with mosaic texture and become coarsening from the rim towards the center (Figure 2(d)).

The upper interval is mainly composed of dolomite, which is gray to light gray (Figures 3(a) and 3(b)). The existence of relict breccias can be observed locally (Figure 3(a)). Pore spaces, produced by dissolution, pervasively occur along the fractures and are partially filled by coarse calcite cements or organic materials (Figures 3(a) and 3(b)). With the utilization of the microscope, the size of dolomite crystals ranges from 5 to 20 μm, characterized by euhedral to subhedral crystals with planar to rectilinear crystal surfaces. Also, it is evident that some dolomite crystals are subject to mild corrosion. Intercrystallite pores are pervasively present and partially occluded by microquartz mineral (Figures 3(c) and 3(d)). Dolomites near fissures are broken into honeycomb pores, while fissures or caves are filled with megacrystal calcite (Figures 3(e) and 3(f)). To current knowledge, core characteristics indicate the typical fluid reforming traces. In this work, efforts have been made to identify the role of fluid in reforming reservoirs by geochemical means.

4. Results

4.1. C-O Isotope Characteristics. The limestones, collected from the Yingshan Formation, Shuntuoguole area, have $\delta^{13}C$ values from -1.25‰ to -1.08‰ VPDB and $\delta^{18}O$ from -7.95‰ to -7.42‰ VPDB. Calcite veins in the limestone have $\delta^{13}C$ values from -2.21‰ to -2.06‰ VPDB and $\delta^{18}O$ from -12.24‰ to -12.08‰ VPDB. Dolomite in Well SHBP1 has $\delta^{13}C$and $\delta^{18}O$ values of -2.14‰ and -7.78‰, respectively. Calcite fillings have $\delta^{13}C$ values from -3.2‰ to -2.6‰ VPDB (average -2.71‰) and $\delta^{18}O$ values from 18.6‰ to 15.4‰ VPDB (average -16.525‰) (Figure 4).

4.2. Sr Isotope Characteristics. The micrite in Yingshan Formation of Shunbei area has a narrow range of $^{87}Sr/^{86}Sr$ ratio, varying from 0.708750 to 0.708792, which is basically consistent with the previously reported ratio of micrite in this area ($^{87}Sr/^{86}Sr$: 0.708899) (Li, Acta Petrolei Sinica). The pack stones yield $^{87}Sr/^{86}Sr$ ratios of 0.70881 to 0.708914, with an average of 0.70885, which is generally consistent with the isotopic ratio of Middle Ordovician age (0.7087~0.7089) [21–23]. Late-stage calcite fillings in fissures have $^{87}Sr/^{86}Sr$ ratios (0.709805~0.710201), greatly higher than those of limestones (Figure 5).

4.3. Fluid Inclusion Microthermometry. Inclusions in dolomite have diameters mostly of <10 μm; therefore, relevant work cannot be conducted. However, massive two-phase inclusions are developed in megacrystal calcite cement, and vapor-liquid two-phase saline inclusions mostly take place in the oriented bands. These inclusions are colorless under transmission light, and they have little typical secondary evolution, with sizes falling in the range of 3 ~ 15 μm, the average value is 8 μm. The minimum homogenization temperature is 124°C, and the maximum temperature exceeds the tolerance of the measuring instrument; thus, homogenization could not be achieved. All the measured temperatures are beyond 230°C. According to inclusion quantity, the average temperature was set slightly higher than 160°C, and the measured main homogenization temperatures were controlled in the 150~160°C or>200°C intervals (Figure 6). The freezing-point temperatures vary from -22.1°C to -8.9°C with an average of -10.9°C. According to the formula

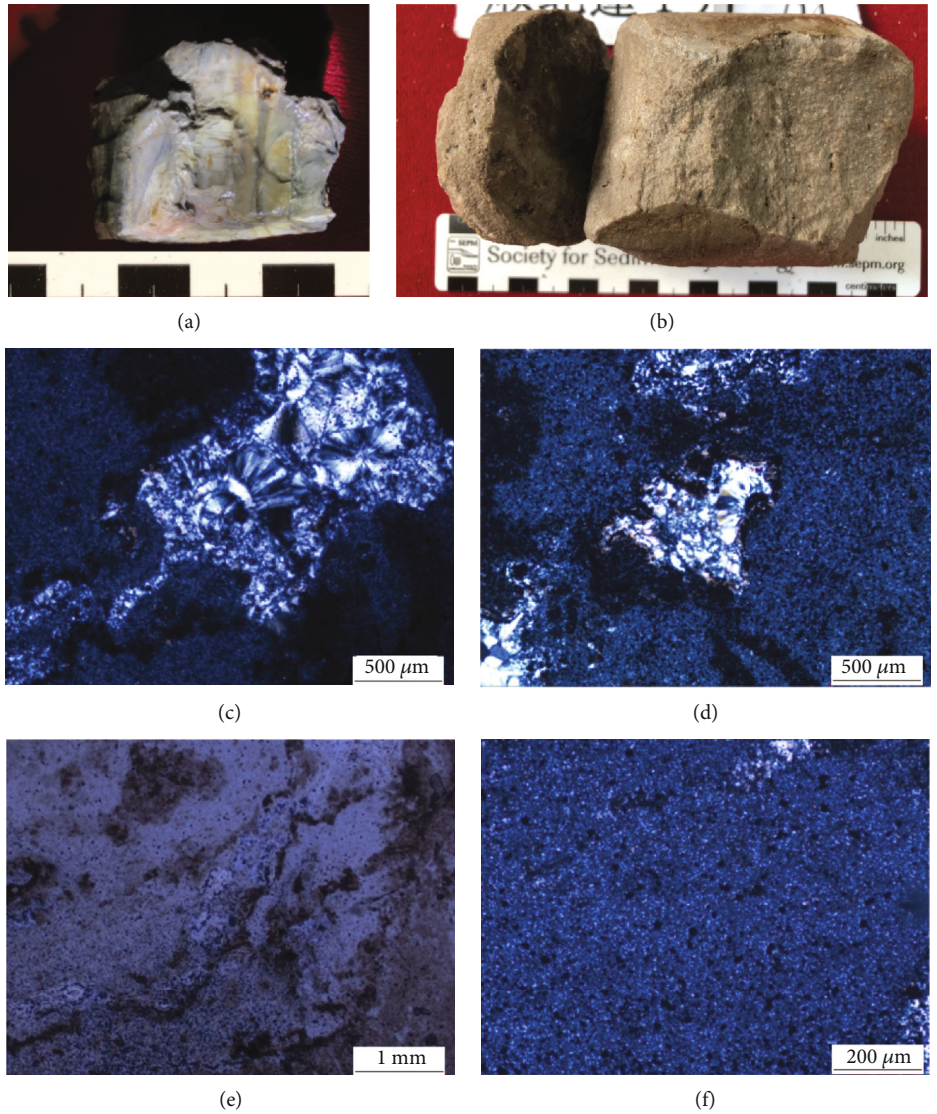

Figure 2: The lower unit characteristics of Well SHBP1. Microscopic/petrographic characteristics of samples in the lower core: (a) Light gray siliceous rock. Silicification develops along fractures, layered siliceous bands, and pyrite, 8455.71-8455.73 m; (b) Light gray siliceous rock. Silica is mainly cryptocrystalline, quartz crystal growth, and residual filling along the fracture wall can be seen on the fracture surface, 8455.73-8455.77 m; (c) Qtz is present as the subhedral quartz crystal, which developed a few pores. Quartz fills the fractures, chalcedony is filled in the fractured-cavity, as observed in microscopic photo of XPL, 8455.74 m; (d) Silicified rock with crystalloblastic texture is composed of microcrystalline quartz and granular quartz, with large intercrystallite pores and reprecipitated calcite cement, 8455.73 m, XPL; (e) Siliceous rocks. It is dominated by microcrystalline quartzite, which consists of microcrystalline quartz and granular quartz with crystalloblastic texture, 8455.72 m, PPL; (f) Siliceous rocks. Partially magnified slice of E, microcrystalline quartz, 8455.72 m, XPL.

[24], the salinities were calculated, ranging from 15.2 to 17.9 wt% NaCl equivalent, with an average of 16.2 wt% NaCl equivalent. In compliance with the definition of fluid inclusion combination [25, 26], it is believed that there are two groups of inclusions. Other than that, considering the temperature difference exceeds 30°C, the hydrothermal fluids may exist.

5. Discussions

According to the aforementioned results, the development characteristics of reservoirs can be summarized. At first, pores are formed along with high-angle fractures and fractured breccias. Then, the reservoir space is composed of dilatant pore-caves along fissures, dolomite intercrystallite (corrosion) pores, and autogenic quartz intercrystallite pores. Aside from that, reservoir development mechanism can be summarized as the interface-controlled faulting-hydrothermal activity. The four main evidences are as follows:

(1) From the macroscopic view, observation of core indicates the fading thermal color along fissures. Moreover, with the help of a microscope, it can be

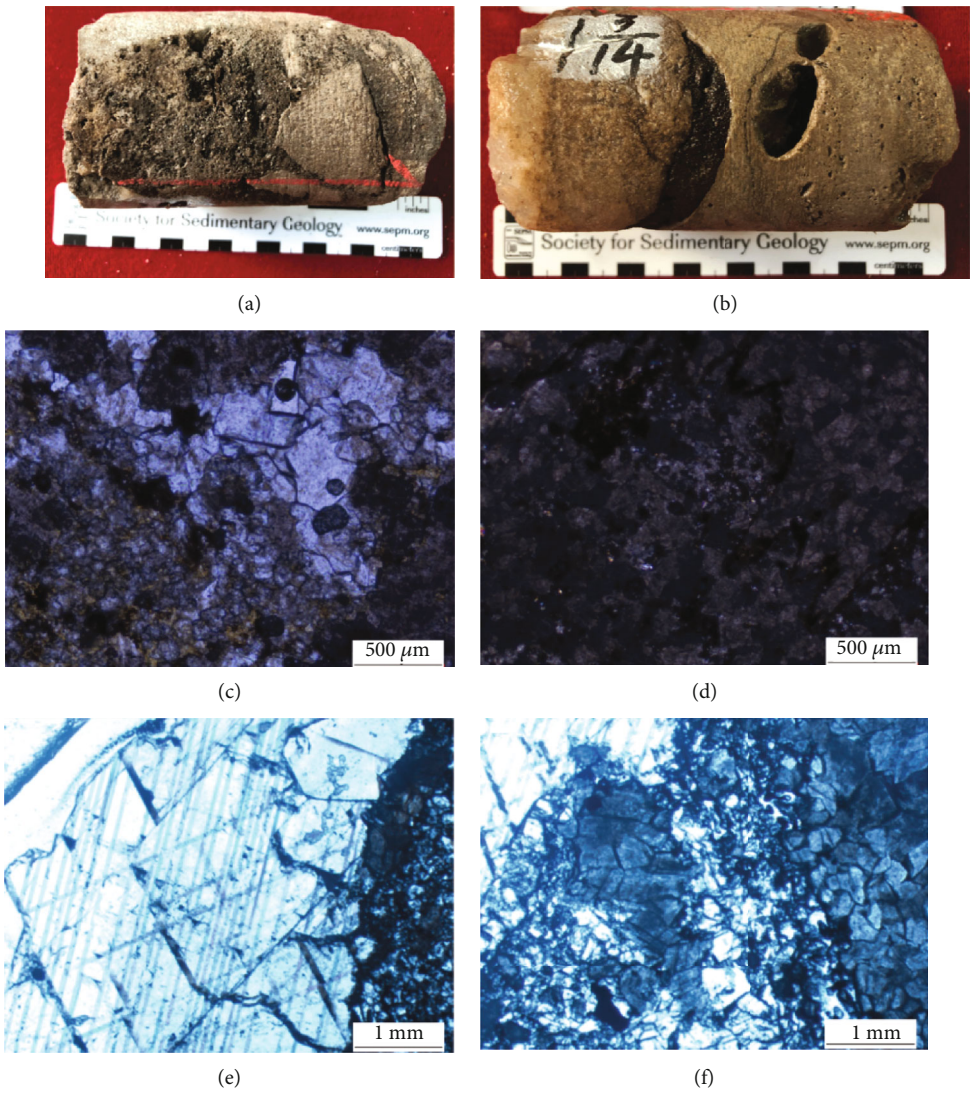

Figure 3: The upper unit characteristics of Well SHBP 1. Microscopic/petrographic characteristics of samples in the upper unit: (a) Gray siliceous dolomite. The dissolution of dolomite and matrix breccia can be found in the fracture, and the dissolution is filled with siliceous and calcite cement, 8453.72-8453.82 m; (b) Fine-medium crystal dolomite. Corrosion pores, 20-50 mm in diameter, are filled with calcite and siliceous parts. There are directional distribution characteristics in the pores, and honeycomb dissolution can be found along the cracks, 8451.12-8451.24 m; (c) Microscopic photo of (a) quartz grains in the intercrystallite of honeycomb dolomite develops the secondary calcite, 8453.74 m, PPL; (d) Siliceous fine-monocrystalline dolomite. Suture Wire Cut Dolomite, 8452.14 m, PPL; (e and f) Powder-fine dolomite. Honeycomb structure, edge of siliceous, and giant crystal calcite, 8450.02 m, PPL.

observed that thermal catacaustic phenomena appear in corrosion pore, and where quartz replacement happens. Thermal color fading is a phenomenon that the rock turns locally or totally shallow (even to white) in color, generally along fissures. This is mainly induced by thermal fluids, activating along fissures and reacting with the surface rocks [27, 28]. Thermal color fading is common in Ordovician carbonate rocks in Tazhong area and mainly displays dark-gray or gray. In addition, thermal color fading is observable in the Silurian sandstone near fissures. Thermal color fading is generally small scaled and merely within several centimeters of two sides of a fissure. As for the case of cores of Well SHBP1, dolomites around fissures experience thermal color fading, and most of them (protolith) are not altered and their color remains grayish white. The alteration only occurs near fissures, and the after-alteration color turns into shallow gray to white

Under thermal activity, a special thermal catacaustic phenomenon is discovered in Silurian sandstones of the Tahe oil/gas field [28]. For lots of sandstone grains, there is one or multiple irregular networked fissures, which are mostly isotropic. Fissures among different grains are generally discontinuous. If the fracturing activity is caused by oriented external force, fissures shall show certain orientation and continuity. The thermal catacaustic phenomenon in sandstone grains is caused by the thermal process, as pressure decreases, hydrothermal fluids swelled rapidly in

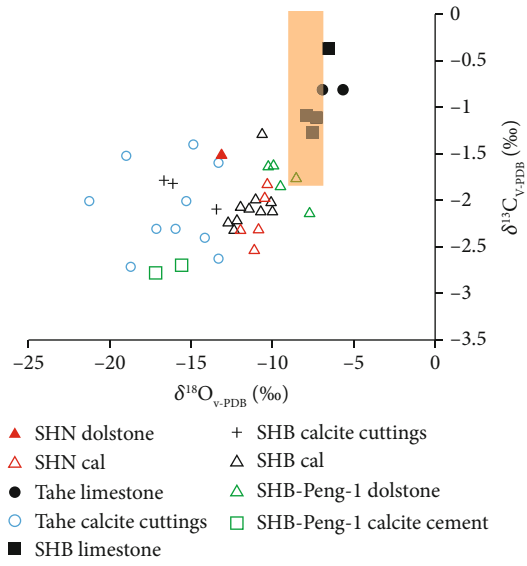

Figure 4: C-O isotopic characteristics.

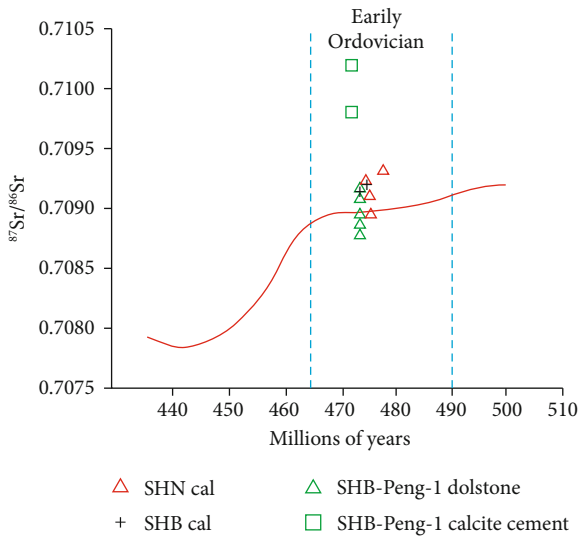

Figure 5: Sr isotopic characteristics.

volume or boiled [29–31]. Honeycomb dissolution pores, observed in Well SHBP1, under a microscope show very similar thermal catacaustic phenomena, fine-crystalline dolomites are densely developed in networked microfissures and filled with automorphic microcrystalline quartz, meanwhile the fissures do not have superior orientation.

(2) A typical hydrothermal mineral assemblage was discovered, denoting the quartz+zeolite. Zeolite is chiefly filled in vesicles and fissures in intermediate–basic volcanic lava, as well as intergranular fissures in volcaniclastic rocks. Zeolite accounts for 5 ~ 32% of the total rock volume, with an average of 18% [32]. Zeolite is generally white, shallow gray, and shallow red. Under a polarizing microscope, zeolite generally occurs as flaky, platy, or needle-like aggregates and displays low negative protuberance. In addition, the crystal surfaces are clear and characterized by gray to white interference colors or a fairly small extinction angle. SEM analysis shows that they occur as columnar or platy-columnar autogenic crystals, with size spanning from 15 to 30 μm. Interpenetration twins are observable, mostly occurring as aggregates filling in pores

On the basis of SEM image observation and spectrum analysis, zeolite occurs in places where honeycomb dissolution pore is developed (Figure 4), with a content of <1%. In the samples here, two shapes of zeolite are observable: (1) the first shape has a high percentage, and the zeolite occurs as aggregates and its outline is close to a rhomb, mainly composed of Ca, Al, and Si; and (2) the second shape is regular and similar to the orthorhombic system of plagioclase, mainly composed of Ca, Al, Si, and O with minor Mg and K. Composition of zeolite is $CaAl_2Si_4O_{12}.6H_2O$, and it is a typical product of high-temperature dolomite, reacting with Si-rich fluid under an alkaline environment.

According to theoretical calculation results (Figure 7), dolomite can react with Si-bearing fluids at 150°C, forming talc [33, 34]. Experimental results of dolomite vs. Si-rich fluids show that dolomite can react with Si-bearing fluids, forming CO_2. Within this experimental temperature range, the solubility of calcite is higher than that of dolomite at the same temperature. According to the aforementioned study, dolomite and calcite can react with Si-bearing fluids at 100~ 200°C, forming CO_2 and Mg/Ca silicates and calcium metasilicate, including talc, zeolite, and other minerals. Besides, in the closed (dolomite–quartz–clay) mineral–water–CO_2 system, clay minerals (smectite) can transform into illite/smectite mixed-layer minerals in alkaline condition.

(3) The measured C-O isotopic values, varying from -1.5 to 0.5‰, are similar with concurrent marine limestone. Additionally, it is discovered that their $\delta^{13}C_{V\text{-}PDB}$ characteristics of the matrix and secondary calcite are different [16, 35, 36], and $\delta^{18}O_{V\text{-}PDB}$ characteristics of the matrix and calcite veins were different from those of seawater at the same time. Carbon isotope is comparatively stable, the C isotope range for surrounding rock of Well SHBP1 is lower than <-1‰ of coeval sea water and higher than <-1‰ of secondary calcite, typical negative bias affected by organic carbon is not discovered. The genesis may be the influence, exerted by high temperature or freshwater. The $\delta^{18}O_{V\text{-}PDB}$ values of the buried dolomites are more negative than those of seawater and marine cements, and more negative than those of contemporaneous dolomites. O isotope shows typical negative bias. Given that $\delta^{13}C$ has proved that organic carbon is lacking, $\delta^{18}O$ of Well SHBP1 shows more typical negative bias characteristics than that of Shunnan area. From the C-O isotope intersection diagram, it can be demonstrated that the quasi-identical formation causes of the dolomite in Well SHBP1 and secondary calcite, further inferring that this characteristic is more affected by

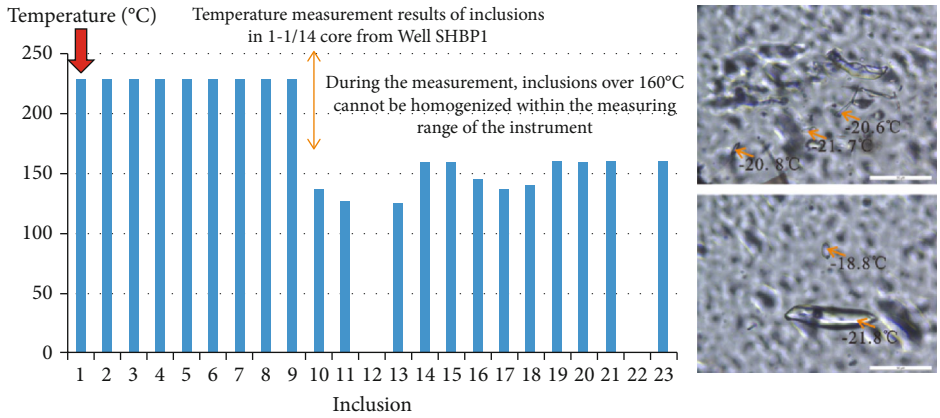

Figure 6: Inclusion temperature characteristics.

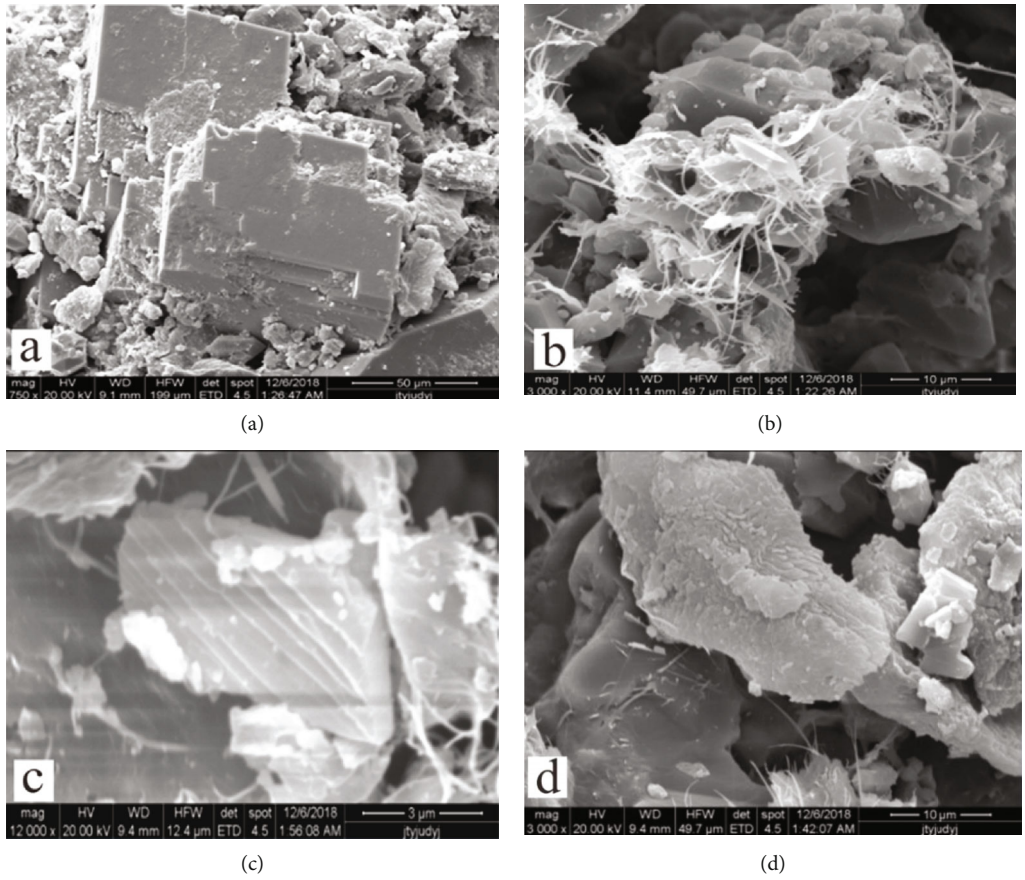

(a) (b) (c) (d)

Figure 7: Characteristics under SEM analysis.

high-temperature fluids and freshwater carbonates, formed by early-stage atmospheric freshwater. *Sr* isotopic characteristics show that bedrock samples from Shunbei area have similar $^{87}Sr/^{86}Sr$ ratio, compared with coeval sea water. In the early Ordovician, the $^{87}Sr/^{87}Sr$ ratio of global seawater ranges from 0.7087 to 0.7092, with an average of 0.7090 [36], and $^{87}Sr/^{86}Sr$ of seawater in the middle Ordovician ranges from 0.70870 to 0.70890. The $^{87}Sr/^{86}Sr$ ratio of the most of the dolomites is generally slightly higher than that of the early-middle Ordovician seawater. $^{87}Sr/^{86}Sr$ ratio indicates the injection of exogenous fluids, but two calcite samples have $^{87}Sr/^{86}Sr$ ratio greatly higher than that of coeval sea water. This phenomenon may be affected by crust-derived Sr, given that C-O isotope analysis shows very

limited atmospheric freshwater characteristics. It is believed that seepage flow poses weak influences on *Sr* isotope. According to the lower formation features, it is inferred that the *Sr* isotopic characteristics are affected by globally widespread lower Cambrian black shale and siliceous rock [37, 38]. Comprehension of C-O isotope characteristics indicate that they are affected by hydrothermal solution

Evidence for the existence of hydrothermal fluids is inclusion temperature measurement. According to the core depth of Well SHBP1 (8450.00~8455.77 m), the ground temperature of the cored location is supposed to be 160°C. Temperature measurement of sparry calcite cement, filled in fissures–caves, indicates that the homogenization temperatures mostly exceed 160°C, and homogenization cannot achieve 230°C evenly. This suggests that the fluid temperature, when corroded magnesium calcium carbonates reprecipitate and form calcium carbonate, is higher by 5°C than that of surface rocks, after siliceous fluid reacting with dolomite. This agrees with the standard of hydrothermal fluid. Therefore, diagenetic, reforming at this position, can be determined to be faulting–hydrothermal fluid reforming.

In fact, similar phenomena are not rare in the middle–lower Ordovician strata of the Tarim Basin. By means of observation, spectrum measurement, formation water Sr isotopic assay of massive rock thin sections from the reservoir interval of the Ordovician, and analysis of fault attributes, the activity characteristics of hydrothermal corrosion fluids and the control on high-quality reservoirs were investigated in-depth. The study implies that hydrothermal minerals are chiefly developed along with fault-associated structural corrosion fissures and pores/caves. Faults are the main pathway for hydrothermal fluid migration and the main controlling factor for forming high-quality reservoirs. Homogenization temperatures, H-O isotopes, and REE composition of fluid inclusions imply that quartz in the lower Paleozoic carbonate rocks was formed by magmatic-hydrothermal fluids. Furthermore, when quartz was precipitated from magma-hydrothermal fluid, carbonate reservoirs were suffered from obvious corrosion. Li (2015) shows hydrothermal alteration and metasomatic silification phenomena in the Ordovician Yingshan Formation and cored interval of Shunnan Well, located at Tarim Basin, and corrosion fissures/caves, loose siliceous limestone/siliceous rock, hydrothermal veins, and coarse quartz clusters are widely developed. Geochemical analyses of core samples indicate that hydrothermal fluids display mixing signatures. The heat was sourced from magmatism, and formation water provided the main fluids, forming medium–low temperature, high-salinity silicified hydrothermal fluids.

As mentioned above, structure-controlled hydrothermal corrosion mainly occurs inside the fractured zone of a strike-slip fault. Due to the seismic wave disturbance, induced by formation fracturing/fault detachment, strong amplitude or "bead-like" strong reflection usually occurs in where fault hydrothermal activity takes place. Inside rock formations, due to fracturing or subsequent hydrofracturing, aroused by thermal brine fluid charging, abundant fissures and breccias are formed in carbonate formations, and wide matrix metasomatic silification happens, enhancing dolomite (or limestone) porosity (molar volume replacement effect). Recharging of episodic thermal brine fluids may dissolve dolomite or limestone, forming drusy caves which are partially filled by megacrystal calcite. If hydrothermal dissolution is strong enough, local collapse of rock formations can occur, thus aggravating the sink of rock formation. Accordingly, hydrothermal dissolution is called as hydrothermal karstification by some scholars [39]. Compared to carbonate wall rocks, these positions usually have more pores, caves, and fissures, while after late-stage fluid reforming, they can turn into potential high-quality reservoirs (Figure 7). Notably, the strong-amplitude abnormal reflector has the width of ~200 m in Shuntuoguole area, and this strong-amplitude reflector can be well recognized by 3D seismic sections, transecting its axis.

In Shunbei oil/gas fields, the geometrical morphology of faults can be drawn according to seismic data amplitude and coherence volume analysis, while porosity and its space variation, inside strong amplitude anomalous bodies, can be precisely depicted by the comprehensive analysis of seismic attributes and logging data. In turn, they can constrain the scope of faulting–hydrothermal action, providing us a more sensible and objective understanding on the reservoir development features. Although multiple methods, including C-O isotope measure, Sr isotope, as well as fluid inclusion analysis, have been applied in this article, the research still suffers some deficiencies. First of all, there are little drilling cores for deep-burial carbonate reservoirs in Tarim Basin. As we know, comprehensive geological knowledge for a specific area roots in the abundant cores, which can provide massive information for analysis. In this article, the majority of the characteristics learn from the case of Well SHBP1, which may result in fairly great uncertainty. Other than that, it is really hard to examine the reliability of the conclusions, summarized on the basis of the experimental data, theoretical analysis, and observations. Finally, applicability activity of the research efforts to the realistic field is still lacking. In light of the above limitations, the authors will continue this research in the future.

6. Conclusions

(1) Based on the detailed core investigation and petrographic examination, two units, including the lower microquartz interval and upper dolomite interval, could be further categorized for the whole core samples. The intense diagenesis of SHBP1 Well was greatly constrained along with the vicinity of faults and/or fractures, indicating the distinctive characteristic of tectonic-controlled hydrothermal alteration

(2) The deep-seated strike-slip faults in the Shunbei area could have provided preferential conduits for hydrothermal fluids migrating upward to the shallow burial carbonates, resulting in intensive dissolution and subsequent cementation. Therefore, fault-controlled hydrothermal reservoirs, characterized

by the strong amplitude in the seismic profile, are widely distribute in the interior of Yingshan Formation

(3) This study provides a useful explanation of tectonic-controlled hydrothermal alteration, which could be helpful to make the exploration strategy, aiming at finding favorable carbonate reservoirs in deeply buried carbonates in the Tarim Basin, particularly in the Shuntuoguole area

Data Availability

Data available on request.

Ethical Approval

On behalf of all the coauthors, the corresponding author states that there are no ethical statements contained in the manuscripts.

Conflicts of Interest

The authors declared no potential conflicts of interest with respect to the research, authorship, an/or publication of this article.

Acknowledgments

We sincerely thank Professor Liu from Peking University and Dr. You from Sinopec Petroleum Exploration and Production Research Institute for their help in the experimental data. The first author acknowledges the Projects of Science and Technology Department of Sinopec (P21033-3) for supporting a part of this work. The research was also supported by NSFC Basic Research Program on Deep Petroleum Resource Accumulation and Key Engineering Technologies (No. U19B6003-02).

References

[1] G. R. Davies and L. B. Smith, "Structurally controlled hydrothermal dolomite reservoir facies: an overview," *AAPG Bulletin*, vol. 90, no. 11, pp. 1641–1690, 2006.

[2] F. J. Lucia, C. Kerans, and J. W. Jennings, "Carbonate reservoir characterization 2007: an integrated approach," *Journal of Petroleum Technology*, vol. 55, no. 6, pp. 70–72, 2003.

[3] S. F. Dong, D. Z. Chen, X. Q. Zhou, Y. Qian, M. Tian, and H. Qing, "Tectonically driven dolomitization of Cambrian to Lower Ordovician carbonates of the Quruqtagh area, northeastern flank of Tarim Basin, north-west China," *Sedimentology*, vol. 64, no. 4, pp. 1079–1106, 2017.

[4] F. Z. Jiao, "Significance of oil and gas exploration in NE strike-slip fault belts in Shuntuoguole area of Tarim Basin," *Oil & Gas Geology*, vol. 38, no. 5, pp. 831–839, 2017.

[5] Y. S. Ma, Z. L. He, P. R. Zhao et al., "A new progress in formation mechanism of deep and ultra-deep carbonate reservoir," *Acta Petrolei Sinica*, vol. 40, no. 12, pp. 1415–1425, 2019.

[6] G. Y. Zhu, X. W. Liu, H. J. Yang et al., "Genesis and distribution of hydrogen sulfide in deep heavy oil of the Halahatang area in the Tarim basin, China," *Journal of Natural Gas Geoscience*, vol. 2, no. 1, pp. 57–71, 2017.

[7] S. Deng, H. Li, Z. Zhang, J. Zhang, and X. Yang, "Structural characterization of intracratonic strike-slip faults in the central Tarim Basin," *AAPG Bulletin*, vol. 103, no. 1, pp. 109–137, 2019.

[8] S. Deng, H. L. Li, Z. P. Zhang, X. Wu, and J. B. Zhang, "Characteristics of differential activities in major strike-slip fault zones and their control on hydrocarbon enrichment in Shunbei area and its surroundings, Tarim Basin," *Oil & Gas Geology*, vol. 39, no. 5, pp. 878–888, 2018.

[9] X. Y. Han, S. Deng, L. J. Tang, and Z. Cao, "Geometry, kinematics and displacement characteristics of strike-slip faults in the northern slope of Tazhong uplift in Tarim Basin: a study based on 3D seismic data," *Marine and Petroleum Geology*, vol. 88, pp. 410–427, 2017.

[10] Y. T. Li, L. X. Qi, and S. N. Zhang, "Characteristics and development mode of the Middle and Lower Ordovician fault-karst reservoir in Shunbei area,Tarim Basin," *Acta Petrolei Sinica*, vol. 40, no. 12, pp. 1470–1484, 2019.

[11] H. B. Qiu, T. Yin, Z. C. Cao et al., "Strike-slip fault and Ordovician petroleum exploration in northern slope of Tazhong Uplift, Tarim Basin," *Marine Origin Petroleum Geology*, vol. 22, no. 4, pp. 44–52, 2017.

[12] Y. Liu, N. Qiu, H. Li, A. Ma, J. Chang, and J. Jia, "Terrestrial heat flow and crustal thermal structure in the northern slope of Tazhong uplift in Tarim Basin," *Geothermics*, vol. 83, p. 101709, 2020.

[13] K. Shang, "Reservoir space characterization and classification of the ultra-deep limestone reservoirs in the northern slope of Central Tarim Basin," *Special Oil & Gas Reservoirs*, vol. 25, no. 5, pp. 65–70, 2018.

[14] K. Shang, N. Guo, and Z. C. Cao, "Main controlling factors of reservoir in Ordovician Yijianfang Formation on the northern slope of middle Tarim Basin," *Marine Origin Petroleum Geology*, vol. 22, no. 1, pp. 39–46, 2017.

[15] D. You, Z. Cao, M. Xu, Y. Qian, S. Wang, and X. Wang, "Genetic mechanism of multi-type dolomite reservoirs in Ordovician Yingshan Formation,Tarim Basin," *Oil & Gas Geology*, vol. 41, no. 1, pp. 92–100, 2020.

[16] D. H. You, J. Han, W. X. Hu et al., "Characteristics and formation mechanisms of silicified carbonate reservoirs in well SN4 of the Tarim Basin," *Energy Exploration & Exploitation*, vol. 36, no. 4, pp. 820–849, 2018.

[17] D. Wei, Z. Gao, C. Zhang, T. Fan, and J. S. Tsau, "Characterization of the deeply buried microporous limestone: case study from the Shunnan area, Tarim Basin, NW China," *Geological Journal*, vol. 55, no. 2, pp. 4920–4935, 2019.

[18] Z. Chai, Z. H. Chen, H. Liu et al., "Light hydrocarbons and diamondoids of light oils in deep reservoirs of Shuntuoguole Low Uplift, Tarim Basin: implication for the evaluation on thermal maturity, secondary alteration and source characteristics," *Marine and Petroleum Geology*, vol. 117, p. 104388, 2020.

[19] Z. Sun, B. Huang, Y. Li, H. Lin, S. Shi, and W. Yu, "Nanoconfined methane flow behavior through realistic organic shale matrix under displacement pressure: a molecular simulation investigation," *Journal of Petroleum Exploration and Production Technology*, 2021.

[20] Z. Sun, S. Wang, H. Xiong, K. Wu, and J. Shi, "Optimal nanocone geometry for water flow," *AICHE Journal*, vol. 68, no. 3, p. e17543, 2021.

[21] R. E. Denison, R. B. Koepnick, W. H. Burke, and E. A. Hetherington, "Construction of the Cambrian and Ordovician seawater $^{87}Sr/^{86}Sr$ curve," *Chemical Geology*, vol. 152, no. 3-4, pp. 325–340, 1998.

[22] L. Hecht, R. Freiberger, H. A. Gilg, G. Grundmann, and Y. A. Kostitsyn, "Rare earth element and isotope characteristics of hydrothermal carbonates: genetic implications for dolomite-hosted talc mineralization at Gopfersgrun," *Chemical Geology*, vol. 155, no. 1-2, pp. 115–130, 1999.

[23] H. R. Qing, C. R. Barnes, D. Buhl, and J. Veizer, "The strontium isotopic composition of Ordovician and Silurian brachiopods and conodonts: relationships to geological events and implications for coeval seawater," *Geochimica et Cosmochimica Acta*, vol. 62, no. 10, pp. 1721–1733, 1998.

[24] R. J. Bodnar, "Revised equation and table for determining the freezing point depression of H_2O-NaCl solutions," *Geochimica et Cosmochimica Acta*, vol. 57, no. 3, pp. 683-684, 1993.

[25] G. X. Chi and H. Z. Lu, "Validation and representation of fluid inclusion microthermometric data using the fluid inclusion assemblage (FIA) concept," *Acta Petrologica Sinica*, vol. 24, no. 9, pp. 1945–1953, 2008.

[26] R. H. Goldstein and T. J. Reynolds, "Systematics of fluid inclusions in diagenetic minerals," *SEPM Short Course*, vol. 31, 1994.

[27] Z. Sun, B. Huang, K. Wu et al., "Nanoconfined methane density over pressure and temperature: wettability effect," *Journal of Natural Gas Science and Engineering*, vol. 99, p. 104426, 2022.

[28] D. Y. Zhu, Z. J. Jin, W. X. Hu, and X. F. Zhang, "Effects of deep fluid on carbonates reservoir in Tarim Basin," *Geological Review*, vol. 54, no. 3, pp. 348–354, 2008.

[29] J. Michel, "Hydrothermal breccias in vein-type ore deposits: a review of mechanisms, morphology and size distribution," *Ore Geology Reviews*, vol. 12, no. 3, pp. 111–134, 1997.

[30] W. J. Phillips, "Hydraulic fracturing and mineralization," *Journal of the Geological Society*, vol. 128, no. 4, pp. 337–359, 1972.

[31] H. Westphal, G. P. Eberli, L. B. Smith, G. M. Grammer, and J. Kislak, "Reservoir characterization of the Mississippian Madison formation, Wind River basin, Wyoming," *AAPG Bulletin*, vol. 88, no. 4, pp. 405–432, 2011.

[32] H. Liang, "Formation and distribution of zeolite in volcanic rock and its effect on reserviors in Santanhu Basin," *Acta Sedimentologica Sinica*, vol. 29, no. 3, pp. 537–543, 2011.

[33] M. B. Holness, "Fluid flow paths and mechanisms of fluid infiltration in carbonates during contact metamorphism: the Beinn an Dubhaich aureole, Skye," *Journal of Metamorphic Geology*, vol. 15, no. 1, pp. 59–70, 1997.

[34] F. Tornos and B. F. Spiro, "The geology and isotope geochemistry of the talc deposits of Puebla de Lillo (Cantabrian Zone, Northern Spain)," *Economic Geology*, vol. 95, no. 6, pp. 1277–1296, 2000.

[35] S. J. Huang, "Carbonate Diagenesis," *Geological Publishing House*, pp. 54–63, 2011.

[36] J. Veizer, D. Ala, K. Azmy et al., "87Sr/86Sr, δ13C and δ18O evolution of Phanerozoic seawater," *Chemical Geology*, vol. 161, no. 1-3, pp. 59–88, 1999.

[37] D. M. Banerjee, M. Schidlowski, F. Siebert, and M. D. Brasier, "Geochemical changes across the Proterozoic-Cambrian transition in the Durmala phosphorite mine section, Mussoorie Hills, Garhwal Himalaya, India," *Palaeogeography Palaeoclimatology Palaeoecology*, vol. 132, no. 1-4, pp. 183–194, 1997.

[38] S. Jiang, J. Yang, H. Ling et al., "Extreme enrichment of polymetallic Ni-Mo-PGE-Au in Lower Cambrian black shales of South China: an Os isotope and PGE geochemical investigation," *Palaeogeography Palaeoclimatology Palaeoecology*, vol. 254, no. 1-2, pp. 217–228, 2007.

[39] D. Z. Chen, "Structure-controlled hydrothermal dolomitization and hydrothermal dolomite reservoirs," *Oil & Gas Geology*, vol. 29, no. 5, pp. 614–622, 2008.

[40] B. U. Haq and S. R. Schutter, "A Chronology of Paleozoic sea-level changes," *Science*, vol. 322, no. 5898, pp. 64–68, 2008.

[41] O. Catuneanu, W. E. Galloway, C. G. S. C. Kendall et al., "Sequence stratigraphy: methodology and nomenclature," *Newsletters on Stratigraphy*, vol. 44, no. 3, pp. 173–245, 2011.

[42] B. Cheng, H. Liu, Z. C. Cao, X. Wu, and Z. Chen, "Origin of deep oil accumulations in carbonate reservoirs within the north Tarim Basin: insights from molecular and isotopic compositions," *Organic Geochemistry*, vol. 139, article 103931, 15 pages, 2020.

[43] R. L. Folk and J. S. Pittman, "Length-slow chalcedony: a new testament for vanished evaporites," *Journal of Sedimentary Research*, vol. 41, pp. 1045–1058, 1971.

[44] F. H. Jiang, "The study of micro pore characteristics on different depth soft soil consolidation by mercury intrusion porosimetry," *Science Technology and Engineering*, vol. 11, no. 31, pp. 7701–7706, 2011.

[45] L. Bing, Z. Rui, K. Qiangfu et al., "An Ordovician carbonate reservoir in strike-slip structures producing form fault-associated fracture systems, 3D seismic region of Northern Shun 8 block," *Carbonates and Evaporites*, vol. 34, no. 3, pp. 545–556, 2019.

[46] M. D. Li, "Thermodynamic discussion on dolomite serpentinization and talcification," *Journal of Mineralogy and Petrology*, vol. 4, pp. 100–104, 1991.

[47] L. Chunyan, L. Changsong, W. Yi, and W. Maobing, "Burial dissolution of Ordovician granule limestone in the Tahe oilfield of the Tarim Basin, NW China, and its geological significance," *Acta Geologica Sinica*, vol. 82, no. 3, pp. 520–529, 2008.

[48] Z. Lu, Y. Li, N. Ye et al., "Fluid inclusions record hydrocarbon charge history in the Shunbei Area, Tarim Basin NW China," *Geofluids*, vol. 2020, Article ID 8847247, 15 pages, 2020.

[49] N. Xinfeng, S. Anjiang, P. Wenqing et al., "Geological modeling of excellent fracture-vug carbonate reservoirs: a case study of the Ordovician in the northern slope of Tazhong palaeouplift and the southern area of Tabei slope, Tarim Basin, NW China," *Petroleum Exploration and Development*, vol. 40, no. 4, pp. 414–422, 2013.

[50] R. Esposito, R. Klebesz, O. Bartoli et al., "Application of the Linkam TS1400XY heating stage to melt inclusion studies," *Central European Journal of Geosciences*, vol. 4, no. 2, pp. 208–218, 2012.

[51] W. Xiaolin, W. Ye, H. Wenxuan et al., "Experimental studies on the interactions between dolomite and SiO2-rich fluids: implications for the formation of carbonate reservoirs," *Geological Review*, vol. 63, no. 6, pp. 1639–1652, 2017.

[52] T. F. Xia, S. L. Chen, and S. J. Li, "Effects of water chemistry on microcracking and compressive strength of granite," *International Journal of Rock Mechanics and Mining Sciences*, vol. 38, no. 4, pp. 557–568, 2001.

[53] Z. Chaojun, J. Chengzao, L. Benliang, L. Xiuyu, and L. Yunxiang, "Ancient karsts and hydrocarbon accumulation in the middle and western parts of the North Tarim uplift, NW China," *Petroleum Exploration and Development*, vol. 37, no. 3, pp. 263–269, 2010.

[54] Z. Jiahui, Z. Rui, W. Yasheng, L. Tianjia, C. Xuemin, and G. Kunzhang, "The origin and distribution of Ordovician Yingshan dolomite on the northern slope of Tazhong area in Tarim Basin," *Carbonates and Evaporites*, vol. 34, no. 3, pp. 507–523, 2019.